

A Database of Teleseismic Shear-Wave Splitting Measurements for the Ordos Block and Adjacent Areas

Lin Liu^{*1,2,3,4}, Stephen S. Gao², Kelly H. Liu², Tu Xue², Yan Jia², and Sanzhong Li^{1,4}

Abstract

The Ordos block of the north China craton and its surrounding regions are affected by the India–Eurasia collision to the southwest and the subduction of the Pacific beneath the Eurasian plates to the east. To provide the foundation for delineating lithospheric deformation and asthenospheric flow beneath this tectonically diverse region, we have created a database of individual shear-wave splitting (SWS) parameters by applying a uniform set of data processing procedures. After automatic data processing and manual checking, a total of 16,705 pairs of well-defined *PKS*, *SKKS*, and *SKS* splitting parameters (fast orientations and splitting times) are obtained from 1225 broadband seismic stations that recorded data between 2007 and 2019. Along the western and southern margins of the Ordos block, the observed seismic anisotropy is attributable to mantle flow deflected by the relatively thick lithospheric root of the Ordos block. A clear back-azimuthal dependence of the fast orientations is observed at some of the stations located in the Alxa block, Ordos block, and Sichuan basin, indicating possible existence of complex anisotropic structures. The new SWS database can be employed by researchers in various fields to study lithospheric deformation and asthenospheric flow beneath the Ordos block and surrounding regions.

Cite this article as Liu, L., S. S. Gao, K. H. Liu, T. Xue, Y. Jia, and S. Li (2022). A Database of Teleseismic Shear-Wave Splitting Measurements for the Ordos Block and Adjacent Areas, *Seismol. Res. Lett.* **XX**, 1–9, doi: [10.1785/0220210310](https://doi.org/10.1785/0220210310).

[Supplemental Material](#)

Introduction

Influenced by the India–Eurasia collision to the southwest and the subduction of the Pacific beneath the Eurasian plates to the east, the geodynamic evolution of the Ordos block and its adjacent areas is complicated and not well understood. The analysis of seismic azimuthal anisotropy is one of the most frequently used approaches to decipher lithospheric deformation and asthenospheric flow (Vinnik *et al.*, 1989; Silver and Chan, 1991). Because of its high lateral resolution relative to most other geophysical techniques, shear-wave splitting (SWS) analysis is arguably the most robust and most commonly used seismological approach to quantify seismic azimuthal anisotropy in the mantle (Ando, 1984; Silver and Chan, 1991; Silver, 1996). It has long been recognized that when a shear wave propagates through an area of azimuthally anisotropic medium, it would split into the fast and slow components with polarization orientations that are orthogonal to each other. Because the presplitting polarization orientation for the *P*-to-*S* converted waves from the core-mantle boundary (XKS, among which the most frequently used phases for SWS analysis are *PKS*, *SKKS*, and *SKS*) is known, they are ideal for delineating seismic azimuthal anisotropy beneath the recording stations (Ando, 1984; Silver and Chan, 1991). The SWS parameters include the polarization orientation of the fast wave (fast

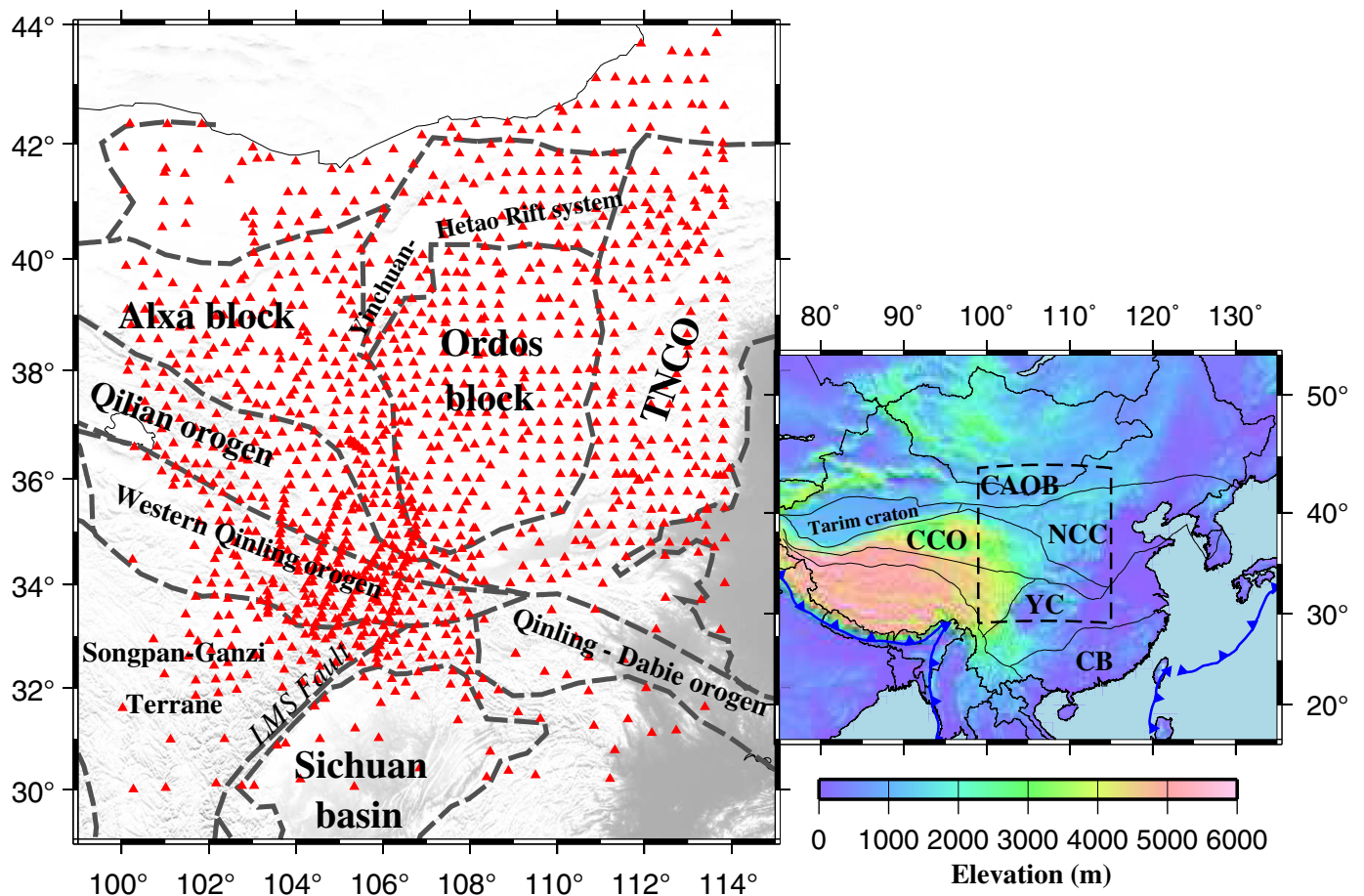
orientation) and the time difference between the fast and slow components (splitting time), respectively (Vinnik *et al.*, 1989; Silver and Chan, 1991; Savage, 1999). The two parameters are routinely utilized to determine the orientation and intensity of anisotropy, which is generally considered as the result of lattice preferred orientation (LPO) of anisotropic minerals (primarily olivine which constitutes more than 65% of the upper mantle) induced by lithospheric deformation and asthenospheric flow (Zhang and Karato, 1995; Katayama and Karato, 2006; Karato *et al.*, 2008).

Under vertically coherent lithospheric deformation with a uniaxial compression, the LPO is perpendicular to the orientation of the maximum compression, and under the influence of asthenospheric flow, the fast orientation is parallel to the direction of simple shear associated with the gradient of plastic

1. Frontiers Science Center for Deep Ocean Multispheres and Earth System, Key Lab of Submarine Geosciences and Prospecting Techniques, MOE, and College of Marine Geosciences, Ocean University of China, Qingdao, China; 2. Geology and Geophysics Program, Missouri University of Science and Technology, Rolla, Missouri, U.S.A., <https://orcid.org/0000-0001-7530-7128> (SSG); <https://orcid.org/0000-0001-7691-9556> (KHL); 3. Department of Geophysics, Stanford University, California, U.S.A.; 4. Laboratory for Marine Mineral Resources, Qingdao National Laboratory for Marine Science and Technology, Qingdao, China

*Corresponding author: lltrc@mst.edu

© Seismological Society of America



flow (Zhang and Karato, 1995; Silver *et al.*, 2001). In addition, in areas with complex anisotropy such as the presence of more than one horizontal anisotropic layers with different LPOs, a systematic azimuthal variation of the individual splitting parameters is observed (Silver and Savage, 1994; Liu and Gao, 2013; Yang *et al.*, 2016).

Although numerous SWS studies have been conducted in the Ordos block and its adjacent areas, the vast majority of the results are presented as station-averaged measurements (Huang *et al.*, 2008; Tang *et al.*, 2010; Zhao and Xue, 2010; Chang *et al.*, 2011, 2017; Li, Wang, and Niu, 2011; Zhao *et al.*, 2011; Yu and Chen, 2016), which are only meaningful for regions with simple anisotropy, that is, a single layer of azimuthal anisotropy with a horizontal axis of symmetry. Because of the fact that the individual splitting parameters may vary as functions of the arriving azimuth of the XKS ray path, in an area with complex anisotropy or spatially varying simple anisotropy, the station-averaged parameters cannot objectively reveal the anisotropic structure (Liu and Gao, 2013; Jia *et al.*, 2021).

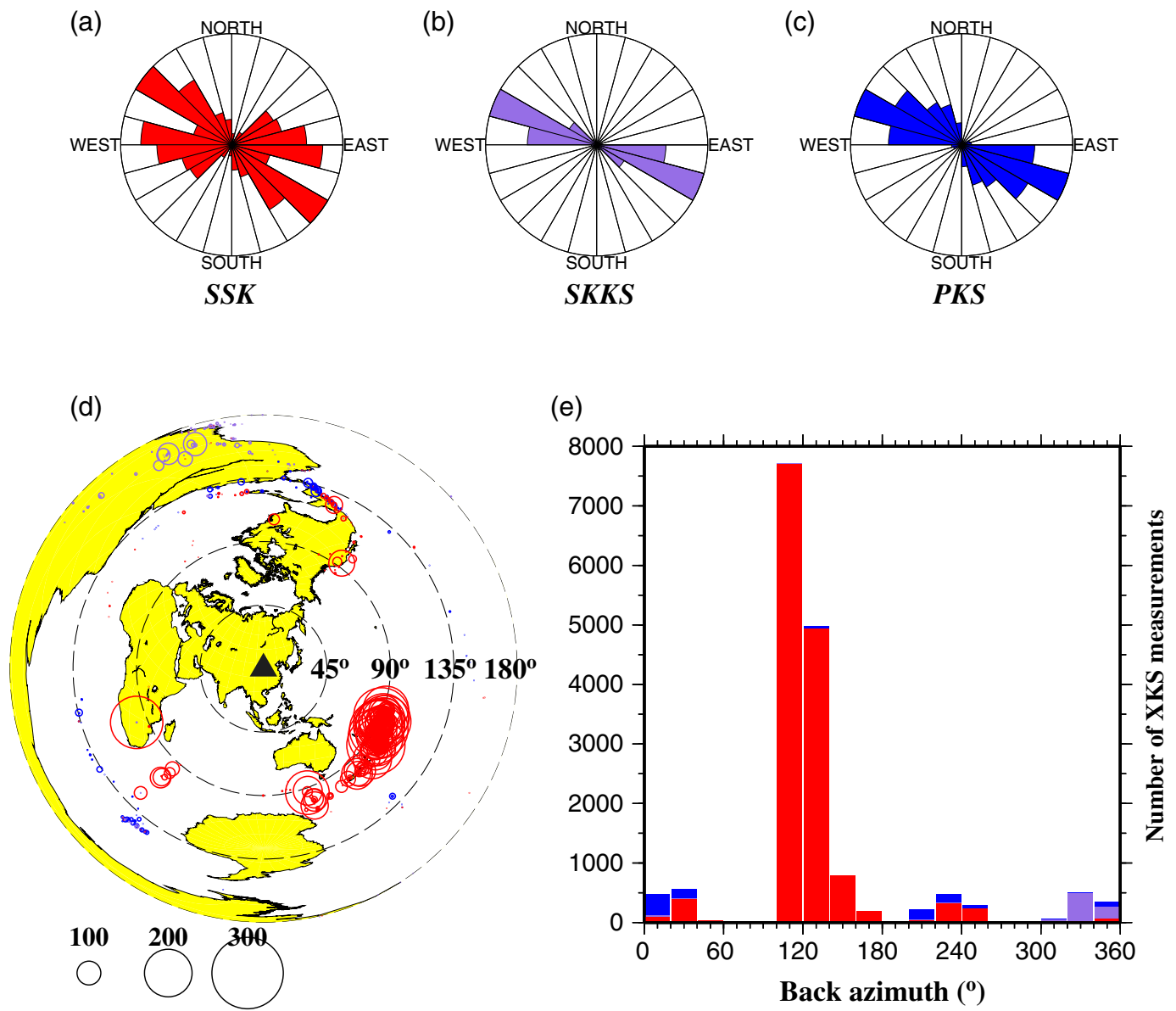
Over the past several years, we have developed a set of procedures to automatically measure, objectively rank, and manually verify the splitting parameters (Liu and Gao, 2013). Uniform databases of both individual and station-averaged SWS parameters using the procedures have been created for the contiguous United States, the Arabia plate, and some other

Figure 1. Map of the study area showing the seismic stations (red triangles) used in the study. The right inset map shows the study area (black dashed line box) and plate boundaries (blue lines with triangles showing the plate convergent directions). CAOB, central Asian orogenic belt; CB, Cathaysia block; CCO, central China orogen; NCC, north China craton; TNCO, Trans-North China orogen; YC, Yangtze craton. The color version of this figure is available only in the electronic edition.

areas (Liu *et al.*, 2014, 2019; Yang *et al.*, 2016, 2017; Kong *et al.*, 2018, 2020; Qaysi *et al.*, 2018). Here, we present a uniform SWS database for the Ordos block and its surrounding regions by applying the well-tested procedures to an outstanding data set recorded by a network of densely spaced broadband seismic stations (Fig. 1). The unprecedented coverage of individual SWS measurements lays the foundation for the estimation of the depth of simple anisotropy and reliable characterization of complex anisotropy models, which cannot be realized using station-averaged splitting parameters.

Data and Method

All the three-component broadband seismic waveform data used in this study area (99°–115° E and 29°–44° N) were obtained from the ChinArray-Himalaya II and III programs and the Data Management Center of the China National



Seismic Network at the Institute of Geophysics, China Earthquake Administration (ChinArray, 2006; Zheng *et al.*, 2010). The recording durations of the 1225 stations are from November 2009 to July 2017 and from July 2007 to August 2019, respectively.

The detailed data processing procedures and the ranking criteria for the measurements are described in our previous studies (Liu *et al.*, 2008, 2019; Liu and Gao, 2013) and are briefly summarized here. To maximize the azimuthal coverage, the epicentral distance ranges that we used for data requesting are 120°–180°, 95°–180°, and 84°–180° for PKS, SKKS, and SKS, respectively, whereas the cutoff magnitude is 5.5. In total, 781 teleseismic earthquakes contributed to at least one measurement, resulting in 16,705 well-defined (ranks A and B using the ranking criteria of Liu *et al.*, 2008) SWS measurements (Fig. 2). The seismograms are detrended and band-pass filtered with corner frequencies of 0.04 and 0.5 Hz, and the ones with a

Figure 2. (a–c) Rose diagrams illustrating the fast orientations obtained using the SKS, SKKS, and PKS phases. (d) An azimuthal equidistant projection map centered at our study area showing seismic events that provided one or more well-defined shear-wave splitting (SWS) measurements. The size of the circles is proportional to the number of XKS measurements from the events. (e) A histogram showing the back-azimuthal distribution of the SWS measurements. The color version of this figure is available only in the electronic edition.

signal-to-noise ratio (SNR) greater than 2.0 on the original radial component are automatically selected. Subsequently, the minimization of transverse energy approach (Silver and Chan, 1991) is utilized to compute the optimal pair of SWS parameters, which corresponds to the minimum energy on the corrected transverse component. All the measurements are automatically ranked as qualities A (outstanding), B

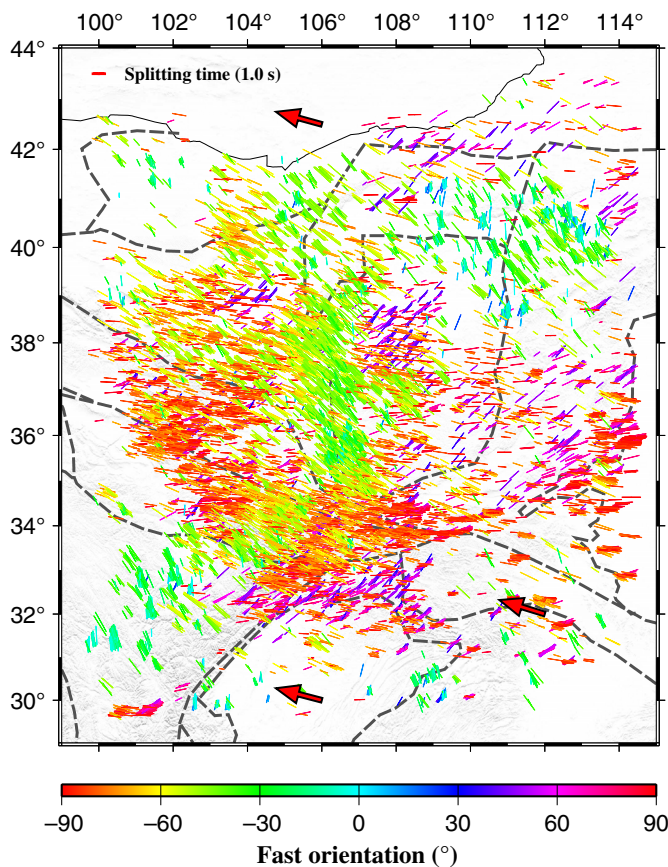


Figure 3. Locations of the 16,705 pairs of XKS SWS measurements plotted at the surface projection of ray-piercing points at 200 km depth. The red arrows represent the absolute plate motion (APM) directions determined by the HS3-NUVEL1A model (Gripp and Gordon, 2002). The color version of this figure is available only in the electronic edition.

(good), C (poor), or N (null) (Liu *et al.*, 2008) according to the SNRs on the four waveforms (the original and corrected radial and transverse components; Liu *et al.*, 2008). This step is followed by manually verifying all the measurements to ensure quality. If necessary, some of the data processing parameters are adjusted, including the beginning and ending times of the XKS window, the band-pass filtering corner frequencies, and the automatically determined quality ranking. The database only includes A- and B-quality measurements.

Database Contents

A total of 16,705 pairs of quality A or B individual splitting parameters are obtained, including 1046 *PKS*, 828 *SKKS*, and 14,831 *SKS* measurements (Figs. 2 and 3). The final database, which consists of the individual splitting parameters (Fig. 3), spatially averaged splitting parameters in 1°-radius circles (Fig. 4), and station-averaged parameters (Fig. 5), are available in the supplemental material to this article (Tables S1–S3). The format of the database is identical to the databases that we produced for the

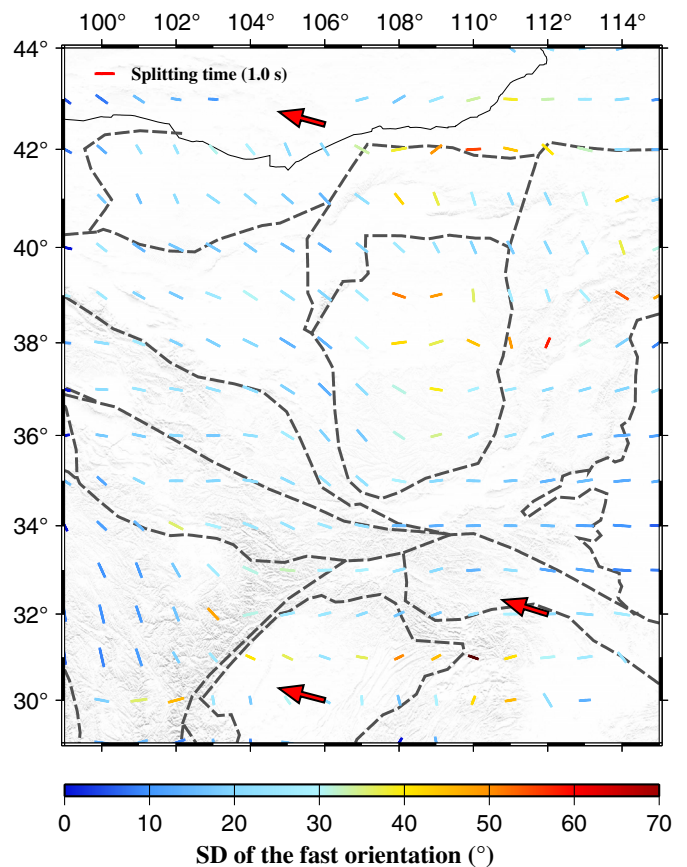


Figure 4. Spatially averaged SWS splitting parameters in consecutive 1°-radius bins. The color of the bars represents the standard deviation (SD) of the fast orientations for each bin. The color version of this figure is available only in the electronic edition.

United States and elsewhere (Liu *et al.*, 2014, 2019; Yang *et al.*, 2016; Qaysi *et al.*, 2018), so that they can be integrated to form a uniform global SWS database in the future. All the stations with high-quality XKS signals resulted in at least one quality A or B measurement. Consequently, null observations simply represent the situation when the fast orientation is parallel or perpendicular to the back azimuth (Silver and Chan, 1991) and are thus not included in the database.

The individual splitting parameters database (Table S1) possesses 17 columns, including station name, phase type, event name, station latitude and longitude, fast orientation, standard deviation (SD) of the fast orientation, splitting time, SD of the splitting time, back azimuth (BAZ) of the event relative to the station, modulo-90° of the BAZ, event latitude and longitude, focal depth, rank of the measurements, and the latitude and longitude of the XKS ray-piercing points calculated at the depth of 200 km.

To produce the spatially averaged SWS parameters (Fig. 4), the individual measurements are grouped into a series of 1°-radius circular bins on the basis of the location of the ray-piercing points at the depth of 200 km, and those with piercing

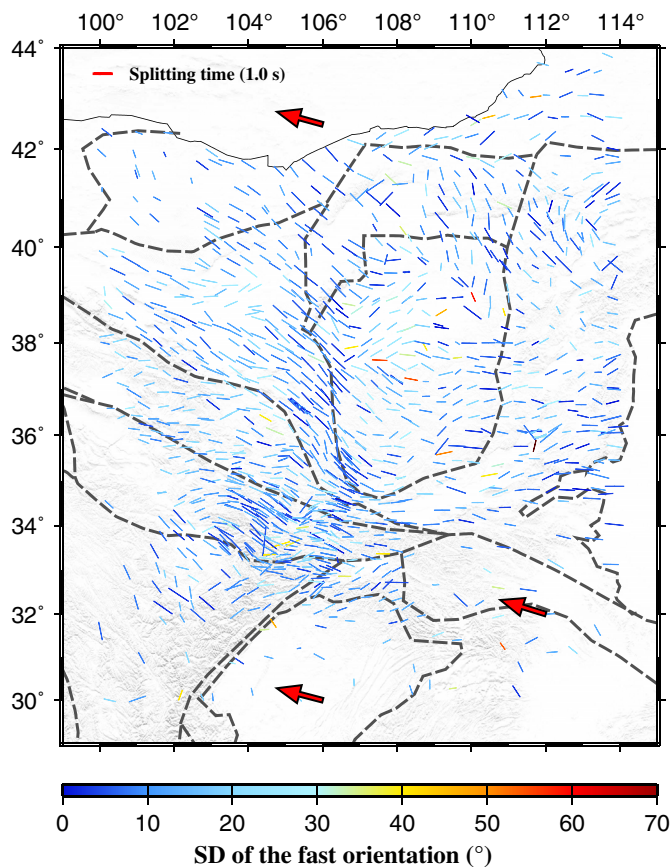


Figure 5. Station-averaged SWS parameters plotted at the locations of the stations. The color of the bars represents the SD of the fast orientations for each station. The color version of this figure is available only in the electronic edition.

points in the same bins are averaged. The distance between neighboring bins is 1° , leading to a certain degree of overlap between neighboring bins. For a given bin, the average fast orientation is calculated using the circular mean of the observed fast orientations in the bin (Mardia and Jupp, 2000), whereas the mean splitting time is computed as the arithmetic average. The database for the spatially averaged splitting parameters (Table S2) contains seven columns (Liu *et al.*, 2014; Yang *et al.*, 2016): the latitude and longitude of the center of the bin, average fast orientation and its SD, average splitting time and its SD, and the number of SWS measurements in the bin.

The station-averaged data set (Fig. 5; Table S3) has eight columns, including the station name, station latitude, station longitude, mean fast orientation, SD of the mean fast orientation, mean splitting time, SD of the splitting time, and the number of individual SWS measurements used to calculate the station averages.

Some First-Order Features of the Observed SWS Parameters

In our study area, the fast orientations have a circular average of $109.7^\circ \pm 36.7^\circ$, whereas the splitting times vary from 0.2

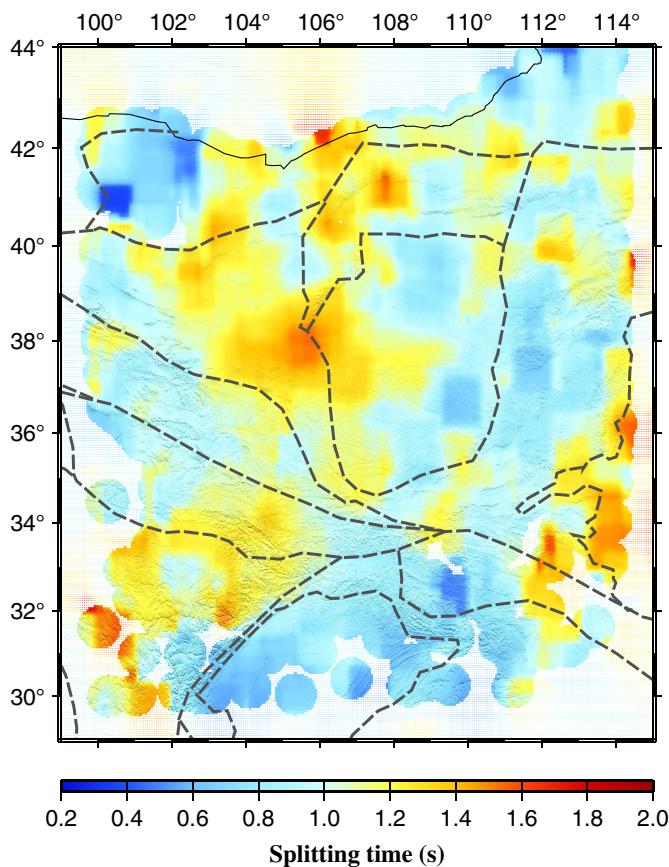


Figure 6. Spatial distribution of splitting times averaged in 1° -radius bins. The color version of this figure is available only in the electronic edition.

to 2.45 s with an arithmetic average of 1.08 ± 0.37 s (Figs. 6 and 7), which is consistent with the global average of 1.0 s for continents (Silver, 1996). Large splitting times are observed in the Alxa block and Songpan–Ganzi Terrane and a small portion of the eastern north China craton (Fig. 6). The station-averaged measurements (Fig. 5) are in general agreement with those obtained by previous SWS studies in this area, most of which only presented their results as station-averaged measurements (whereas this study presents both station-averaged and individual measurements). In particular, the Qilian and western Qinling orogens are dominated by northwest–southeast fast orientations, which are generally consistent with results from previous investigations (Tang *et al.*, 2010; Chang *et al.*, 2011, 2017; Li, Wang, and Niu, 2011; Yu and Chen, 2016). In addition, along the western and southern margins of the Ordos block, the northwest–southeast and east–west fast orientations are subparallel to the surface geological features and in agreement with those obtained from previous studies (Huang *et al.*, 2008; Tang *et al.*, 2010; Chang *et al.*, 2011; Li, Wang, and Niu, 2011; Yu and Chen, 2016). In the Yinchuan–Hetao rift system and the Trans-North China orogen, which were poorly sampled by

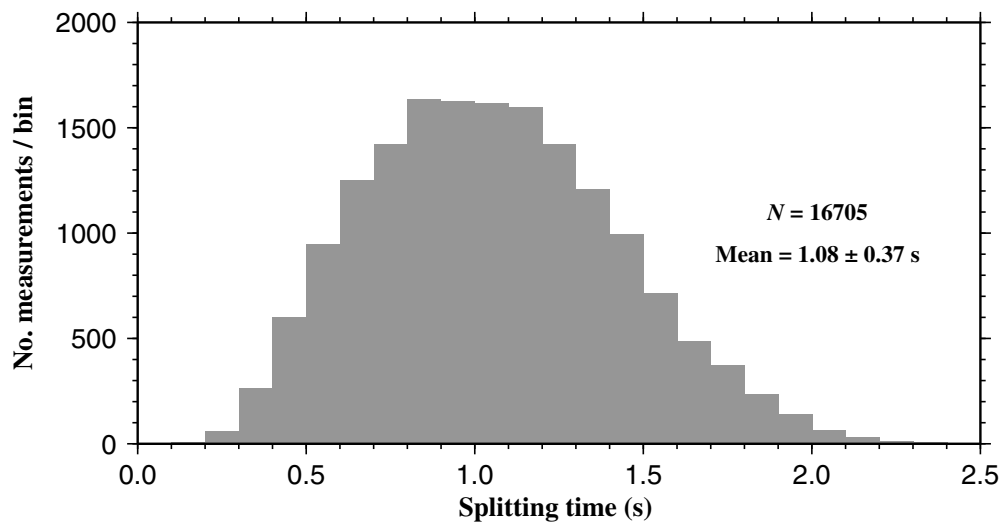


Figure 7. Histogram showing the distribution of XKS splitting times in the study area.

previous SWS studies, the fast orientations are nearly north-south in the north and turn to east-west in the south. The fast orientations in the Songpan–Ganzi Terrane are mostly north-northwest–south-southeast, which are consistent with previous studies in this area (Tang *et al.*, 2010; Li, Wang, and Niu, 2011; Zhao *et al.*, 2011; Yu and Chen, 2016; Chang *et al.*, 2017).

Discussions

Although the vast majority of SWS studies utilize a single frequency band that is broad enough to include most of the XKS energy and at the same time reduce the level of ambient noises, some studies explore possible frequency dependence of the resulting splitting parameters (e.g., Marson-Pidgeon and Savage, 1997; Wirth and Long, 2010; Kong *et al.*, 2020). In general, statistically significant frequency dependence, mostly in the form of a negative correlation between the frequency and the splitting time, is found in tectonically active areas, especially subduction zones (e.g., Kong *et al.*, 2020, for the Sumatra subduction zone). We investigate possible frequency dependence of the splitting parameters by using two low-pass corner frequencies (e.g., Wirth and Long, 2010). The first is 0.04 Hz, and the other is 0.15 Hz. As demonstrated by the examples shown in Figure 8, the resulting splitting parameters are statistically identical for almost all the measurements.

Laboratory and observational investigations indicate that seismic azimuthal anisotropy is mostly induced by asthenospheric flow and vertically coherent deformation of the lithosphere (Vinnik *et al.*, 1989; Silver and Chan, 1991; Zhang and Karato, 1995; Silver, 1996). In areas dominated by vertically coherent deformation, the observed fast orientations are expected to be predominantly parallel to the strike of the orogenic belt and perpendicular to the direction of maximum horizontal shortening (Silver and Chan, 1991); and in areas where asthenospheric flow is the prevailing anisotropy-forming

process, the fast orientations generally align with the flow direction (Vinnik *et al.*, 1989). Although the fast orientations in most parts of the study area are consistent with the direction of the absolute plate motion (APM; Gripp and Gordon, 2002; Fig. 4), significant discrepancies exist between the two in some regions (e.g., the northern Ordos block and the northeast corner of the Tibetan plateau; Fig. 9). These discrepancies, together with the fact that most of the fast orientations are not in agreement with the dominant strike of the major tectonic boundaries

(Fig. 3), suggest that lithospheric fabrics are not a major contributor for the observed azimuthal anisotropy in those regions. Therefore, simple anisotropic models, such as vertically coherent deformation of the crust and upper mantle and APM-related asthenospheric flow, may not be sufficient to interpret the observed SWS measurements in some portions of the study area. In addition, the fast orientations at most stations in the Alxa and Ordos blocks and the Sichuan basin show periodic back-azimuthal variations and large standard deviations in the splitting parameters (Figs. 4 and 5). These features suggest the possible existence of anisotropy structures that are more complex than the assumption of simple anisotropy, that is, a single anisotropic layer with a horizontal axis of symmetry (Silver, 1996). Therefore, station-averaged measurements obtained by most previous investigations (Huang *et al.*, 2008; Tang *et al.*, 2010; Zhao and Xue, 2010; Chang *et al.*, 2011, 2017; Li, Wang, and Niu, 2011; Zhao *et al.*, 2011; Yu and Chen, 2016) may not objectively reflect the true anisotropic structure in the areas with possible existence of complex anisotropy.

The Qilian and western Qinling orogens show smaller splitting times than the western and southern margins of the Ordos block (Fig. 6). Such a pattern is inconsistent with a dominantly lithospheric origin of the observed anisotropy advocated by some previous SWS studies (e.g., Chang *et al.*, 2017). This is because orogenic belts have usually experienced stronger lithospheric deformation than the adjacent stable blocks, and consequently greater splitting times are expected in the former areas if lithospheric deformation is the main source of the observed anisotropy. The larger splitting times observed in the marginal areas of the Ordos block can be explained by contributions from a mantle flow system moving around the deep lithospheric root of the Ordos block (Yu and Chen, 2016; Zhang *et al.*, 2019, 2022), a model that is

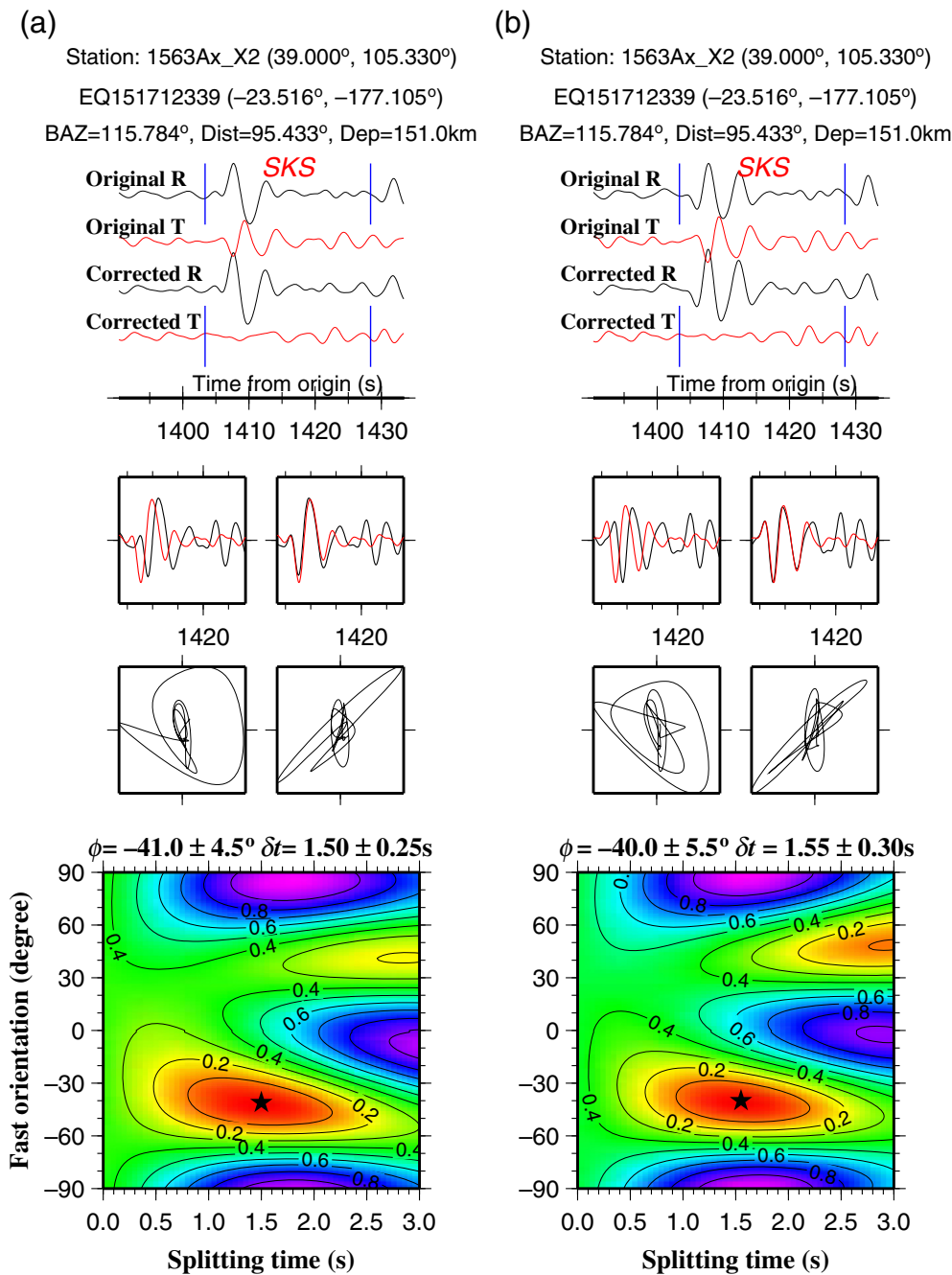


Figure 8. Examples of SWS measurements from event EQ151712339 at station 1563Ax_X2 with different corner frequencies of (a) 0.04–0.5 Hz and (b) 0.15–0.5 Hz. The top plots show original and corrected radial and transverse components of seismograms. The central plots present resulting fast (red) and slow (black) waveforms and particle motion patterns. The bottom plots are contours of normalized energy on the corrected transverse component, in which the black stars mark the optimal pair of splitting parameters corresponding to the minimum energy. The color version of this figure is available only in the electronic edition.

similar to what has been proposed for the southern and eastern margins of the North American craton (Fouch *et al.*, 2000; Refayee *et al.*, 2014; Yang *et al.*, 2017). Finally, the fast orientations in the Songpan–Ganzi Terrane are greatly different from the APM direction (Fig. 9) and are attributable to

lithospheric deformation and mantle flow associated with the India–Tibet collision, as proposed by previous SWS studies in the area (Li and Wu, *et al.*, 2011; Liu *et al.*, 2019).

Conclusions

We have created a uniform data set of individual SWS parameters for the western and central north China craton using an unprecedented set of broadband seismic data in terms of spatial and azimuthal coverages. In total, 16,705 pairs of well-defined individual measurements recorded by 1225 seismic stations were obtained. The large database of individual, station-averaged, and areal-averaged splitting measurements provides a solid foundation for in-depth investigation of the structure, evolution, and dynamics of the lithosphere and asthenosphere beneath the tectonically diverse Ordos block and the adjacent areas. It can be readily utilized for recognizing and characterizing complex anisotropy, estimating the depth of the source of anisotropy, and comparing the spatial and azimuthal variations of the individual splitting parameters with predictions from various geodynamic modeling studies.

Data and Resources

Seismograms used in this study were obtained from the Data Management Center of the China Seismic Array (<http://www.chinarraydmc.cn/dataApply/index>)

and the China National Seismic Network (<http://www.seisdmc.ac.cn/>) at the Institute of Geophysics, China Earthquake Administration. The supplemental material includes all the measurements involved in the database. All the well-defined data products can be downloaded from <https://web.mst.edu/~lltrc/Ordos-SWS-SI.zip>. All websites were last accessed in August 2019.

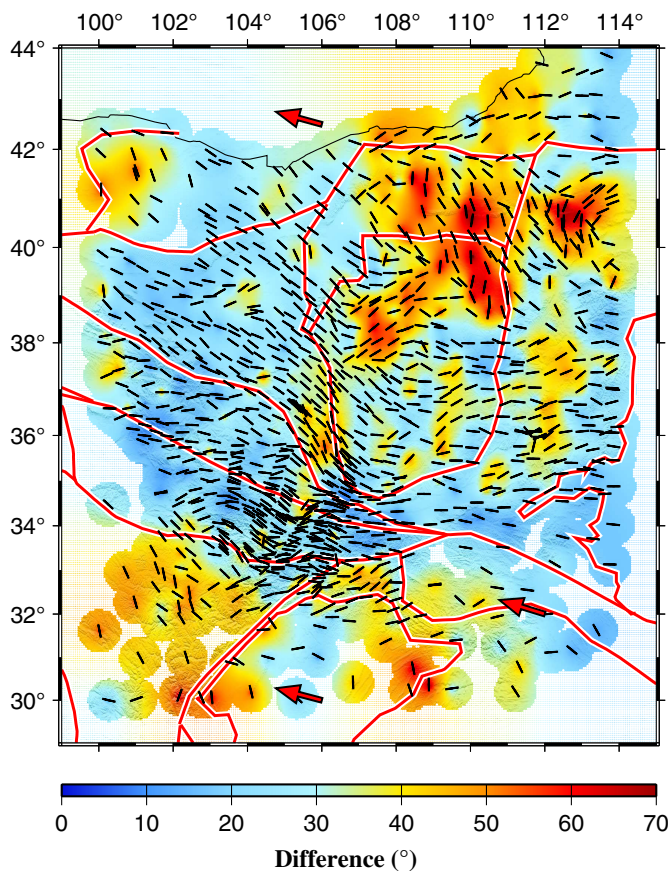


Figure 9. Absolute difference between the observed fast orientations and the APM direction (red arrows). The color version of this figure is available only in the electronic edition.

Declaration of Competing Interests

The authors acknowledge that there are no conflicts of interest recorded.

Acknowledgments

The authors thank the Data Management Center of the China Seismic Array and the China National Seismic Network at the Institute of Geophysics, China Earthquake Administration, for providing the data used in the study. Constructive reviews from two anonymous reviewers, Editor Allison Bent, and an associate editor significantly improved the manuscript. This study is supported by a fellowship from the Ocean University of China to L. L., the National Natural Science Foundation of China (Grant Number 91958214) and the Taishan Scholars Climbing Program (Grant Number tspd20210305) to S. L., and the United States National Science Foundation (Grant Numbers 1830644 and 1919789) to K. L. and S. G.

References

Ando, M. (1984). ScS polarization anisotropy around the Pacific ocean, *J. Phys. Earth* **32**, 179–195, doi: [10.4294/jpe1952.32.179](https://doi.org/10.4294/jpe1952.32.179).
 Chang, L., Z. Ding, C. Wang, and L. M. Flesch (2017). Vertical coherence of deformation in lithosphere in the NE margin of the Tibetan plateau using GPS and shear-wave splitting data, *Tectonophysics* **699**, 93–101, doi: [10.1016/j.tecto.2017.01.025](https://doi.org/10.1016/j.tecto.2017.01.025).

Chang, L., C. Wang, and Z. Ding (2011). Upper mantle anisotropy in the Ordos block and its margins, *Sci. China Earth Sci.* **54**, no. 6, 888–900.
 ChinArray (2006). China seismic array waveform data: China earthquake administration, doi: [10.12001/ChinArray](https://doi.org/10.12001/ChinArray). Data.
 Fouch, M. J., K. M. Fischer, E. M. Parmentier, M. E. Wysession, and T. J. Clarke (2000). Shear wave splitting, continental keels, and pattern of mantle flow, *J. Geophys. Res.* **105**, 6255–6275, doi: [10.1029/1999JB900372](https://doi.org/10.1029/1999JB900372).
 Gripp, A. E., and R. G. Gordon (2002). Young tracks of hotspots and current plate velocities, *Geophys. J. Int.* **150**, 321–361, doi: [10.1046/j.1365-246X.2002.01627.x](https://doi.org/10.1046/j.1365-246X.2002.01627.x).
 Huang, Z., M. Xu, L. Wang, N. Mi, D. Yu, and H. Li (2008). Shear wave splitting in the southern margin of the Ordos block, north China, *Geophys. Res. Lett.* **35**, no. 19, L19301, doi: [10.1029/2008GL035188](https://doi.org/10.1029/2008GL035188).
 Jia, Y., K. H. Liu, F. Kong, L. Liu, and S. S. Gao (2021). A systematic investigation of piercing point dependent seismic azimuthal anisotropy, *Geophys. J. Int.* **227**, no. 3, 1496–1511, doi: [10.1093/gji/ggab285](https://doi.org/10.1093/gji/ggab285).
 Karato, S., H. Jung, I. Katayama, and P. Skemer (2008). Geodynamic significance of seismic anisotropy of the upper mantle: New insights from laboratory studies, *Annu. Rev. Earth Planet. Sci.* **36**, 59–95, doi: [10.1146/annurev.earth.36.031207.124120](https://doi.org/10.1146/annurev.earth.36.031207.124120).
 Katayama, I., and S. I. Karato (2006). Effect of temperature on the B-to C-type olivine fabric transition and implication for flow pattern in subduction zones, *Phys. Earth Planet. In.* **157**, nos. 1/2, 33–45, doi: [10.1016/j.pepi.2006.03.005](https://doi.org/10.1016/j.pepi.2006.03.005).
 Kong, F., S. S. Gao, K. H. Liu, J. Zhang, and J. Li (2020). Seismic anisotropy and mantle flow in the Sumatra subduction zone constrained by shear wave splitting and receiver function analyses, *Geochem. Geophys. Geosys.* **21**, e2019GC008766, doi: [10.1029/2019GC008766](https://doi.org/10.1029/2019GC008766).
 Kong, F., J. Wu, L. Liu, K. H. Liu, J. Song, J. Li, and S. S. Gao (2018). Azimuthal anisotropy and mantle flow underneath the southeastern Tibetan plateau and northern Indochina peninsula revealed by shear wave splitting analyses, *Tectonophysics* **747**, 68–78, doi: [10.1016/j.tecto.2018.09.013](https://doi.org/10.1016/j.tecto.2018.09.013).
 Li, J., X. Wang, and F. Niu (2011). Seismic anisotropy and implications for mantle deformation beneath the NE margin of the Tibet plateau and Ordos plateau, *Phys. Earth Planet. In.* **189**, nos. 3/4, 157–170, doi: [10.1093/gji/ggab154](https://doi.org/10.1093/gji/ggab154).
 Li, Y., Q. Wu, F. Zhang, Q. Feng, and R. Zhang (2011). Seismic anisotropy of the northeastern Tibetan plateau from shear wave splitting analysis, *Earth Planet. Sci. Lett.* **304**, 147–157, doi: [10.1016/j.epsl.2011.01.026](https://doi.org/10.1016/j.epsl.2011.01.026).
 Liu, K. H., and S. S. Gao (2013). Making reliable shear-wave splitting measurements, *Bull. Seismol. Soc. Am.* **103**, no. 5, 2680–2693, doi: [10.1785/0120120355](https://doi.org/10.1785/0120120355).
 Liu, K. H., A. Elsheikh, A. Lemnifi, U. Purevsuren, M. Ray, H. Refayee, B. Yang, Y. Yu, and S. S. Gao (2014). A uniform database of teleseismic shear wave splitting measurements for the western and central United States, *Geochem. Geophys. Geosys.* **15**, 2075–2085, doi: [10.1002/2014GC005267](https://doi.org/10.1002/2014GC005267).
 Liu, K. H., S. S. Gao, Y. Gao, and J. Wu (2008). Shear wave splitting and mantle flow associated with the deflected Pacific slab beneath northeast Asia, *J. Geophys. Res.* **113**, no. B1, doi: [10.1029/2007JB005178](https://doi.org/10.1029/2007JB005178).

- Liu, L., S. S. Gao, K. H. Liu, S. Li, S. Tong, and F. Kong (2019). Toroidal mantle flow induced by slab subduction and rollback beneath the eastern Himalayan syntaxis and adjacent areas, *Geophys. Res. Lett.* **46**, no. 20, 11,080–11,090, doi: [10.1029/2019GL084961](https://doi.org/10.1029/2019GL084961).
- Mardia, K. V., and P. Jupp (2000). *Directional Statistics*, Second Ed., John Wiley and Sons Ltd., Chichester, United Kingdom.
- Marson-Pidgeon, K., and M. K. Savage (1997). Frequency-dependent anisotropy in Wellington, New Zealand, *Geophys. Res. Lett.* **24**, 3297–3300, doi: [10.1029/97GL03274](https://doi.org/10.1029/97GL03274).
- Qaysi, S., K. H. Liu, and S. S. Gao (2018). A database of shear-wave splitting measurements for the Arabian plate, *Seismol. Res. Lett.* **89**, no. 6, 2294–2298, doi: [10.1785/0220180144](https://doi.org/10.1785/0220180144).
- Refayee, H. A., B. B. Yang, K. H. Liu, and S. S. Gao (2014). Mantle flow and lithosphere-asthenosphere coupling beneath the southwestern edge of the North American craton: Constraints from shear-wave splitting measurements, *Earth Planet. Sci. Lett.* **402**, 209–220, doi: [10.1016/j.epsl.2013.01.031](https://doi.org/10.1016/j.epsl.2013.01.031).
- Savage, M. K. (1999). Seismic anisotropy and mantle deformation: What have we learned from shear wave splitting? *Rev. Geophys.* **37**, 65–106, doi: [10.1029/98RG02075](https://doi.org/10.1029/98RG02075).
- Silver, P. G. (1996). Seismic anisotropy beneath the continents: Probing the depths of geology, *Ann. Rev. Earth Planet. Sci.* **24**, 385–432, doi: [10.1146/annurev.earth.24.1.385](https://doi.org/10.1146/annurev.earth.24.1.385).
- Silver, P. G., and W. W. Chan (1991). Shear wave splitting and subcontinental mantle deformation, *J. Geophys. Res.* **96**, no. B10, 16,429–16,454, doi: [10.1029/91JB00899](https://doi.org/10.1029/91JB00899).
- Silver, P. G., and M. K. Savage (1994). The interpretation of shear-wave splitting parameters in the presence of two anisotropic layers, *Geophys. J. Int.* **119**, no. 3, 949–963, doi: [10.1111/j.1365-246X.1994.tb04027.x](https://doi.org/10.1111/j.1365-246X.1994.tb04027.x).
- Silver, P. G., S. S. Gao, K. H. Liu, and the Kaapvaal Seismic Group (2001). Mantle deformation beneath southern Africa, *Geophys. Res. Lett.* **28**, 2493–2496, doi: [10.1029/2000GL012696](https://doi.org/10.1029/2000GL012696).
- Tang, Y., Y. J. Chen, Y. V. Fu, H. Wang, S. Zhou, E. Sandvol, J. Ning, Y. Feng, and M. Liu (2010). Mantle anisotropy across the southwestern boundary of the Ordos block, north China, *Earthq. Sci.* **23**, no. 6, 549–553.
- Vinnik, L. P., V. Farra, and B. Romanowicz (1989). Azimuthal anisotropy in the Earth from observations of SKS at Geoscope and NARS broadband stations, *Bull. Seismol. Soc. Am.* **79**, no. 5, 1542–1558, doi: [10.1016/0009-2541\(89\)90139-3](https://doi.org/10.1016/0009-2541(89)90139-3).
- Wirth, E., and M. D. Long (2010). Frequency-dependent shear wave splitting beneath the Japan and Izu-Bonin subduction zone, *Phys. Earth Planet. In.* **181**, 141–154, doi: [10.1016/j.pepi.2010.05.006](https://doi.org/10.1016/j.pepi.2010.05.006).
- Yang, B. B., K. H. Liu, H. H. Dahm, and S. S. Gao (2016). A uniform database of teleseismic shear-wave splitting measurements for the western and central United States: December 2014 update, *Seismol. Res. Lett.* **87**, no. 2A, 295–300, doi: [10.1785/0220150213](https://doi.org/10.1785/0220150213).
- Yang, B. B., Y. Liu, H. Dahm, K. H. Liu, and S. S. Gao (2017). Seismic azimuthal anisotropy beneath the eastern United States and its geodynamic implications, *Geophys. Res. Lett.* **44**, no. 6, 2670–2678, doi: [10.1002/2016GL071227](https://doi.org/10.1002/2016GL071227).
- Yu, Y., and Y. J. Chen (2016). Seismic anisotropy beneath the southern Ordos block and the Qinling-Dabie orogen, China: Eastward Tibetan asthenospheric flow around the southern Ordos, *Earth Planet. Sci. Lett.* **455**, 1–6, doi: [10.1016/j.epsl.2016.08.026](https://doi.org/10.1016/j.epsl.2016.08.026).
- Zhang, S., and S. Karato (1995). Lattice preferred orientation of olivine aggregates deformed in simple shear, *Nature* **375**, 774–777, doi: [10.1038/375774a0](https://doi.org/10.1038/375774a0).
- Zhang, Y., L. Chen, Y. Ai, and M. Jiang (2019). Lithospheric structure beneath the central and western north China craton and adjacent regions from S-receiver function imaging, *Geophys. J. Inter.* **219**, no. 1, 619–632, doi: [10.1093/gji/ggz322](https://doi.org/10.1093/gji/ggz322).
- Zhang, C., Z. Guo, Y. Yu, T. Yang, and Y. J. Chen (2022). Distinct lithospheric structures of the Ordos block and its margins from P and S receiver functions and its implications for the cenozoic lithospheric reworking, *Geophys. Res. Lett.* e2021GL097680, doi: [10.1029/2021GL097680](https://doi.org/10.1029/2021GL097680).
- Zhao, L., and M. Xue (2010). Mantle flow pattern and geodynamic cause of the north China craton reactivation: Evidence from seismic anisotropy, *Geochem. Geophys. Geosys.* **11**, Q07010, doi: [10.1029/2010GC003068](https://doi.org/10.1029/2010GC003068).
- Zhao, L., T. Zheng, G. Lu, and Y. Ai (2011). No direct correlation of mantle flow beneath the north China craton to the India-Eurasia collision: Constraints from new SKS wave splitting measurements, *Geophys. J. Int.* **187**, no. 2, 1027–1037, doi: [10.1111/j.1365-246X.2011.05201.x](https://doi.org/10.1111/j.1365-246X.2011.05201.x).
- Zheng, X. F., Z. X. Yao, J. H. Liang, and J. Zheng (2010). The role played and opportunities provided by IGP DMC of China National Seismic Network in Wenchuan earthquake disaster relief and researches, *Bull. Seismol. Soc. Am.* **100**, 2866–2872, doi: [10.1785/0120090257](https://doi.org/10.1785/0120090257).

Manuscript received 28 October 2021

Published online 8 April 2022